MALAYSIAN JOURNAL OF ANALYTICAL SCIENCES

Journal homepage: https://mjas.analis.com.my/

**Research Article**

# Biopolymer-assisted synthesis of bifunctional mesoporous $K_2O$ beads for one-pot esterification–transesterification in biodiesel production

Nor Badariah Talib[1], Ong Hui Shan[1], Jegthiswary Suresh[1], Khairil Juhanni Abd Karim[1], Nurrulhidayah Salamun[1], Salmiah Jamal Mat Rosid[2], and Susilawati Toemen[1*]

[1] Department of Chemistry, Faculty of Science, Universiti Teknologi Malaysia, 81310 UTM Skudai, Johor, Malaysia
[2] UniSZA Science and Medicine Foundation Centre, Universiti Sultan Zainal Abidin, Gong Badak Campus, 21300, Kuala Nerus, Terengganu, Malaysia

[*]Corresponding author: susilawatitoemen@utm.my

Received: 24 September 2025; Revised: 1 March 2026; Accepted: 7 April 2026; Published: 30 April 2026

**Abstract**

Transesterification is the preferred process for producing biodiesel, a sustainable fuel similar to fossil diesel. Potassium-based catalysts are highly valued in transesterification due to their remarkable basicity, well supported by numerous studies.In this study, mesoporous metal oxide (MMO) beads were synthesised using potassium precursor and biopolymers as templates to guide the formation of porous morphology with improved accessibility of active sites. Chitosan and alginate were evaluated, with chitosan demonstrating superior performance due to its strong affinity for potassium ions and abundant functional groups. Field Emission Scanning Electron Microscopy (FESEM) revealed a brain-like, wrinkled morphology of interconnected folds, which suggests mesoporosity properties. Nitrogen adsorption analysis supported this, showing an average pore diameter of 17.75 nm, and a pore volume of 0.039 $cm^3/g$. X-ray diffraction (XRD) confirmed active basic center ($K_2O$, $K_2O_2$) and the presence of $K_2CO_3 \cdot 1.5H_2O$, which acts both as a structural binder and acidic center. Hammett analysis suggests bifunctionality, with basicity of 1.346 mmol/g and acidity of 1.515 mmol/g. Under optimised synthesis conditions; K:chitosan monomer ratio of 4:1, 0.5 v/v% acetic acid, calcined at 700 °C for 2 h, the catalyst achieved a biodiesel yield of 95.17% from waste cooking oil (WCO), demonstrating the effectiveness of the synthesised catalysts in biodiesel production.

**Keywords:** biopolymer, mesoporous bead catalyst, biodiesel, bifunctional catalyst, potassium catalyst

## Introduction

The growth of the global population and improved living condition has urge high demand for fuel consumption and this has led to a shortfall in energy provision [1]. Despite new oil reservoir discoveries, fossil fuels are now not dependable as they are costly and promptly drained assets. Biodiesel has been recognised worldwide for its compatible physicochemical properties as well as conventional diesel fuels [2]. Transesterification of oil into fatty acid methyl ester (FAME) is the most efficient pathway for biodiesel production. Numbers of researcher have all studied and proved the high performance of potassium solid base catalyst towards the transesterification process.

Potassium-based catalysts are frequently synthesised in powder form without supporting materials due to their simple preparation and high basicity, which makes them effective for transesterification. However, despite their widespread use, unsupported potassium-based catalysts often suffer from poor recyclability, which remains a key challenge. This is mainly due to the leaching of active potassium species into the reaction medium, as well as agglomeration and loss of surface area during repeated cycles. Consequently, their catalytic performance decreases over time, limiting their reusability and practical application [2].To address this, morphing the catalyst into a bead could aid in separation from the reaction media. To improve the stability of the catalyst that is resistant to metal leaching, the catalyst can be modified into a mesoporous metal oxide (MMO) bead. MMO have a well-defined porous structure with an interconnected network of channels. The presence of these organised pores gives provides excellent performance and stability in catalysis [3].

MMO can be achieved by applying an organic template that acts as a scaffold or mould around which the catalyst is. The template will then be decomposed after thermal treatment, leaving only MMO [4]. Among many templates, polymers can be recognised as an outstanding candidate, due to their ability to connect with metals. Chitosan, an abundant biopolymer contain both hydroxyl and amino groups on its backbone. Therefore, fabrication with metal such as potassium is highly possible due to its reactivity. Due to the intramolecular and intermolecular physical crosslinking, the chitosan will be gelated into spherical particles upon exposure to basic sodium hydroxide [5]. Alginate is an exopolymer of natural origin, containing carboxylic acid in its moiety that allows it to form complexes with cationic metal ions [6]. Potassium-alginate bead can be achieved through exchange between potassium cation with sodium ions attached to the carbonyl group of the alginic acid [7]. Chitosan and alginate are both biodegradable and naturally occurring biopolymers generated from renewable sources. Furthermore, because they are biodegradable, they may be quickly broken down and eliminated from the environment, decreasing any environmental concerns. Chitosan and alginate beads provide encapsulation adaptability since the size, shape, and porosity of the beads may be easily changed throughout the preparation process [7,8]. The polymer molecule's aggregation is strong due to intramolecular and intermolecular physical crosslinking, ensuring an organised scaffold framework for the MMO structural stability.

Therefore, this project aims to fabricate a biopolymer as a template for a mesoporous potassium oxide bead catalyst. The synthesised catalysts were characterised using Differential Scanning Calorimetry (DSC), Thermogravimetric analysis (TGA), XRD, Hammet indicator, $N_2$ adsorption-desorption (NA) and FESEM analyses. The effects of various parameters, including different potassium modifications, calcination temperatures, and potassium precursors, were also studied

## Materials and Methods

### Materials

For this study, potassium nitrate ($KNO_3$), and potassium chloride (KCl) were purchased from Sigma-Aldrich and Merck for the preparation of mesoporous potassium oxide-biopolymer catalyst. For the polymer template, chitosan from shrimp (low molecular weight, 75 % acetylated) and alginic acid sodium salt were purchased from Sigma-Aldrich. Next for the synthesis of potassium-chitosan bead, glacial acetic acid (99%) and sodium hydroxide (NaOH) were purchased from Merck and Qrec. For the transesterification reaction, methanol ($CH_3OH$), n-hexane and methyl nonadecaonate, which are used as reactant, solvent and internal standard, respectively, were purchased from Sigma-Aldrich. Waste cooking oil (WCO) was collected from the student cafeteria around UTM.

### Synthesis of catalyst

Chitosan beads were prepared via ionic gelation, adapted from reference [9] with modifications for potassium incorporation. 4 g of chitosan were dissolved in 200 mL of 0.5 v/v% acetic acid. Then, 10.01 g of $KNO_3$ (monomer to metal ratio 4:1) was added and stirred for 3 h at room temperature, followed by an overnight resting to remove bubbles. The solution was added dropwise into 1 M NaOH under stirring to form spherical beads, which were then equilibrated for 5 h. After repeated washing and drying at 60°C overnight, the beads were calcined at 700 °C for 2 h.

Alginate beads were prepared following reference [10] with modifications for potassium incorporation. 4 g of sodium alginate were mixed with 200 mL of deionised water at 60 °C to form a gel. The cooled mixture was extruded dropwise into 30% (w/v) $KNO_3$ solution under stirring for 6 h to form beads via ion exchange. The beads were repeatedly washed, dried at 60 °C overnight, and calcined at 700 °C for 2 h. Both catalysts were further optimised by varying synthesis parameters, including potassium precursor (KCl), and calcination temperature (600 °C ) achieve the best catalytic performance.

The labelling used in this study distinguishes between synthesis stages. Before calcination, the materials are referred to as A-B, where A denotes the potassium precursor, and B is the biopolymer used. While after calcination, they are renamed as $K_2O$-XT, where X represent biopolymer used and template, and T is abbreviated from "templated".

### Catalyst characterization

Thermal analysis was performed using a Mettler Toledo TG-DSC STARe system with dry air and nitrogen purge gases flowing at 50 mL/min, over a temperature range of 25–300°C at a heating rate of 10°C/min. DSC measurements utilised alumina crucibles, and TGA was conducted with 15–20 mg catalyst samples heated from 60 to 1000°C at 15°C/min under a nitrogen flow of 50 mL/min using a TGA-DTG 851 Mettler Toledo analyser. The best catalyst in terms of the highest biodiesel yield will undergo characterization analysis, namely XRD, FESEM and Hammet analysis. XRD analysis of the catalyst crystal structure was performed with a Siemens D5000 Diffractometer (2θ range: 20°–80°, scan rate 3°/min) and SmartLab Studio II software. Morphology of the catalyst was examined via FESEM

Hitachi SU8020 with platinum-coated samples under 5.0 kV. Nitrogen adsorption-desorption analysis for pore characteristics was conducted using Micromeritics ASAP 2010 after grinding and outgassing catalyst samples at 120°C for 2 h. Basicity was measured by Hammett indicator titration with benzene carboxylic acid in methanol, while acidity was determined by titration with n-butylamine in acetonitrile, following established methods [11,12].

**Transesterification reaction**

10 g of oil was heated in a 50 mL round-bottom flask at 65 °C. Then, 0.6 g of catalyst and 6.6 g of methanol (6 w/w% catalyst, methanol to oil ratio 18:1) were added, and the mixture was stirred under reflux for 3 h. After cooling to room temperature, the biodiesel was separated. Biodiesel mass conversion was calculated using Equation (1).

Conversion (%) =
(weight of biodiesel / weight of raw oil,g) x 100 (1)

Biodiesel was analysed using gas chromatography-flame ionisation detection (GC-FID) with a DB-HeavyWAX column (30 m × 0.255 mm × 0.25 µm), helium as carrier gas, and programmed oven temperatures starting at 60 ºC with staged ramps to 240 ºC. Injector and detector temperatures were set at 250 ºC. Biodiesel was diluted with 10,000 ppm internal standard, and 1 µL was injected. Purity was calculated following the EN 14103 standard using methyl nonadecanoate as the internal standard (IS) using Equation (2). The final yield of biodiesel will be calculated as in Equation (3).

Purity (%) =
(Σ FAME area / IS area) x (IS weight / weight of sample ) x 100 (2)

Yield (%) = (conversion x purity) / 100 (3)

To achieve the best biodiesel yield, three reaction conditions were optimised which were the methanol to oil ratio, the reaction temperature and the time. The reaction conditions were optimised by varying the methanol to oil ratio from 12:1 to 24:1, reaction temperature from 60 to 70 °C, and reaction time from 2 to 4 h to maximise biodiesel yield. To ensure the reliability of the optimisation results, all experiments were conducted in triplicate, and the reported values represent average results.

**Results and Discussion**

**Differential scanning calorimetry and thermal gravimetric analysis**

**Figure 1** presents the DSC and TGA results for $KNO_3$-Chitosan and KCl-Alginate catalysts, revealing their thermal behaviour and stability. **Figure 1a** shows the DSC curves of dried $KNO_3$-Chitosan and KCl-Alginate catalysts, in a nitrogen atmosphere at 10 °C/min revealed the endothermic nature of the fragmentation. The DSC data show distinct thermal events for each catalyst, with $KNO_3$-Chitosan exhibiting water loss at 129°C, glycosidic bond breakage at 186°C, and main polymer chain disintegration at 223°C [13,14,15]. In contrast, KCl-Alginate experiences water loss earlier at 90°C, thermal cleavage of carboxylate groups at 200°C, and depolymerisation of its polysaccharide network at 272°C [16,17].

Correspondingly, TGA (**Figure 1b**) curves demonstrate three stages of weight loss. For $KNO_3$-Chitosan, the initial stage (100–250°C) involves 32% weight loss due to moisture evaporation; the second stage (250–725°C) shows 18% loss associated with polymer decomposition and potassium salt breakdown into potassium oxide; the final stage (725–925°C) involves a further 30% loss attributed to binder decomposition [14,15,18]. KCl-Alginate follows a similar pattern but with less moisture loss (10%) in the first stage and a more substantial 71% weight loss in the third stage (700–1000°C), signifying collapse of structural integrity [19,20]. Both catalysts maintain structural integrity below 800°C, suggesting that calcination at or below this temperature effectively preserves the catalyst framework. Notably, $KNO_3$-Chitosan exhibits more gradual and less severe weight loss during the high-temperature stages, indicating superior thermal stability and resilience compared to KCl-Alginate.

**Effect of catalyst synthesis parameter**

**Figure 2a** illustrates the significant impact of potassium modification and calcination time on biodiesel yield for both chitosan and alginate catalysts. Notably, chitosan calcined at 700 °C achieved a dramatic yield increase to approximately 95%, compared to much lower yields without calcination or at 600 °C, while alginate also showed improvement but to a lesser extent. Calcination at 600 °C may not sufficiently develop the catalyst's active sites or induce complete phase transformation, resulting in a less well-defined structure and lower catalytic activity. In contrast, calcination at 700 °C promotes more thorough decomposition of precursors and crystallisation of potassium species, creating a more stable and accessible active site structure that leads to higher biodiesel yield.

**Figure 2b** presents the effect of different potassium precursors on yield, with both catalysts calcined at 700 °C for 2 h. Chitosan with $KNO_3$ yielded around 95%, markedly higher than with KCl (~29%), whereas alginate showed a higher yield with KCl (~80%)

compared to $KNO_3$ (~28%). Across both precursors, chitosan consistently outperformed alginate. This superior catalytic performance of chitosan can be attributed to its amine ($-NH_2$) and hydroxyl (-OH) groups, which establish stronger ionic and hydrogen bonding with potassium ions, facilitating more uniform incorporation and dispersion of active species throughout the polymer matrix. This is further enhanced by the preparation method, where the potassium precursor is mixed directly with chitosan dissolved in acetic acid prior to ionic gelation, promoting homogeneity in potassium distribution. Conversely, alginate's carboxylate groups bind potassium ions mainly via ionic exchange during bead formation, where sodium alginate solution is dropped into potassium solution [21]. This results in less uniform, surface-concentrated potassium incorporation, limiting catalyst accessibility and activity. Therefore, the difference in functional groups and synthesis pathways leads to more catalytically accessible and stable potassium species in chitosan than in alginate, explaining the observed superiority in biodiesel yield.

**Catalyst characterization**

The calcined $KNO_3$-Chitosan templated catalyst, hereafter referred to as $K_2O$-ChiT, was selected for detailed characterization based on its superior biodiesel production performance shown in **Figure 2**. The catalyst was calcined at 700 °C for 2 h to achieve optimal phase formation and activity. **Figure 3a** shows the XRD of $K_2O$-ChiT calcine at 700 °C for 2 h. The XRD pattern of the catalyst was compared to reference patterns from the Inorganic Crystal Structure Database (ICSD). No peaks for $KNO_3$ were detected, indicating its decomposition to potassium oxides upon calcination at 700 °C. The catalyst displays distinct peaks corresponding to cubic $K_2O$ ($2\theta$ = 31.2°, 32.2°, 32.8°, 37.8°, 51.0°, 55.1°), hexagonal $K_2O$ ($2\theta$ = 29.1° to 53.6°), and orthorhombic $K_2O_2$ ($2\theta$ = 29.0°, 39.8°, 56.9°), suggesting partial oxidation to potassium peroxide.

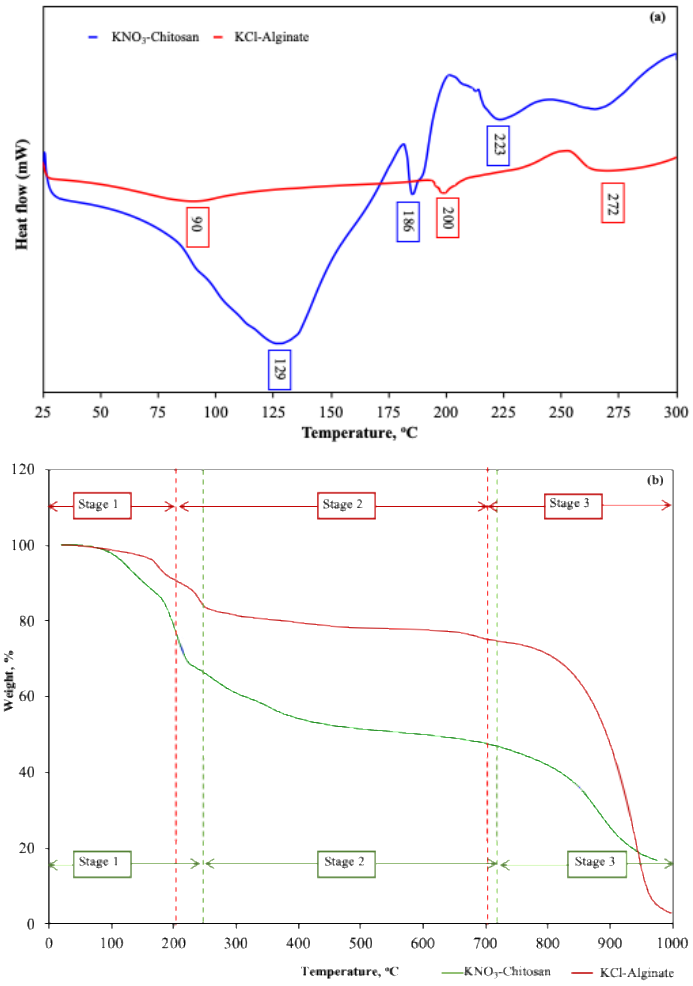


**Figure 1**. (a) DSC curve and (b) TGA curve of dried $KNO_3$-Chitosan and KCl-Alginate

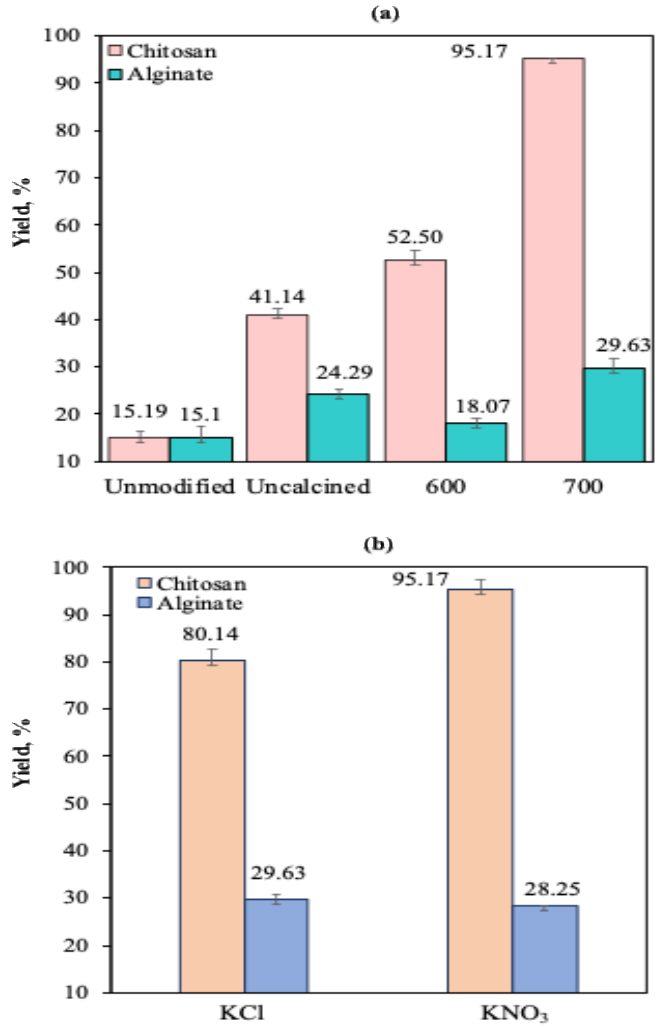


**Figure 2**. The effect of (a) potassium modification and calcination time, (b) potassium precursor towards biodiesel yield

Monoclinic potassium carbonate sesquihydrate ($K_2CO_3 \cdot 1.5H_2O$) peaks ($2\theta$ = 29.5° to 55.7°) indicate its role as a binder with prominent peaks observed at $2\theta$ = 32.2°, 32.5°,32.8°, 33.3° and 33.6° . $K_2O$ formed during calcination can react with $CO_2$ released from chitosan decomposition to produce anhydrous $K_2CO_3$. Upon cooling and exposure to atmospheric moisture, partial hydration of $K_2CO_3$ may occur, leading to the formation of stable hydrated carbonate species such as $K_2CO_3 \cdot 1.5H_2O$ [22]. The presence of multiple potassium phases reflects complex structural transformations during calcination. The potassium compounds in the $K_2O$-ChiT catalyst serve as the active sites that efficiently catalyse the transesterification of waste cooking oil, leading to a high biodiesel yield, as demonstrated in **Figure 2**.

**Figure 3b** shows the FESEM image revealing a brain-like morphology with interconnected ridges and folds. Visible pore channels emphasise the catalyst's internal porous framework, formed during calcination by $CO_2$ and water release from chitosan decomposition, which produces $K_2CO_3 \cdot 1.5H_2O$ as confirmed by XRD. This hydrated phase creates a loosely connected network that acts as a binder, preserving the catalyst's structural integrity after template decomposition. Such porosity increases catalytic activity by expanding the surface area and enhancing reactant-product diffusion to active sites, while the binder maintains mechanical stability, preventing collapse and ensuring long-term catalyst durability and accessibility for improved performance.

The average pore diameter of the catalyst is 17.75 nm with a total pore volume of 0.039 $cm^3/g$, as shown in Table 1, which supports the porous structure observed in the FESEM analysis. Although the pore diameter falls within the mesoporous range (2–50 nm), the

measured BET surface area is relatively low (6.784 $m^2/g$), indicating limited surface development. This may be attributed to structural densification during carbonisation and potassium incorporation, which reduces the overall surface area while maintaining mesoporous pore dimensions. The presence of pore channels can still facilitate the diffusion of reactants and products to the active sites, contributing to catalytic performance.

Hammett titration results (**Table 1**) indicate the presence of both acidic and basic sites, suggesting bifunctional acid–base characteristics of the catalyst, with acidity and basicity values of 1.515 mmol/g and 1.346 mmol/g, respectively. The coexistence of these sites is beneficial for biodiesel production, as acidic sites may promote esterification of free fatty acids, while basic sites facilitate transesterification of triglycerides. To verify the occurrence of esterification in the one-pot system, the free fatty acid (FFA) content and total acid number (TAN) were measured before and after the reaction. A significant reduction in FFA from 5.76% to 0.24% and TAN from 11.52 to 0.4816 mg KOH/g was observed, confirming that esterification had taken place. In parallel, the high biodiesel yield (95.17%) indicates effective transesterification. However, the distribution and strength of acid–base sites are inferred from Hammett analysis. In addition, the presence of pore channels may aid in the mass transfer of reactants and products. These combined factors are likely to contribute to the high biodiesel yield observed under optimised conditions.

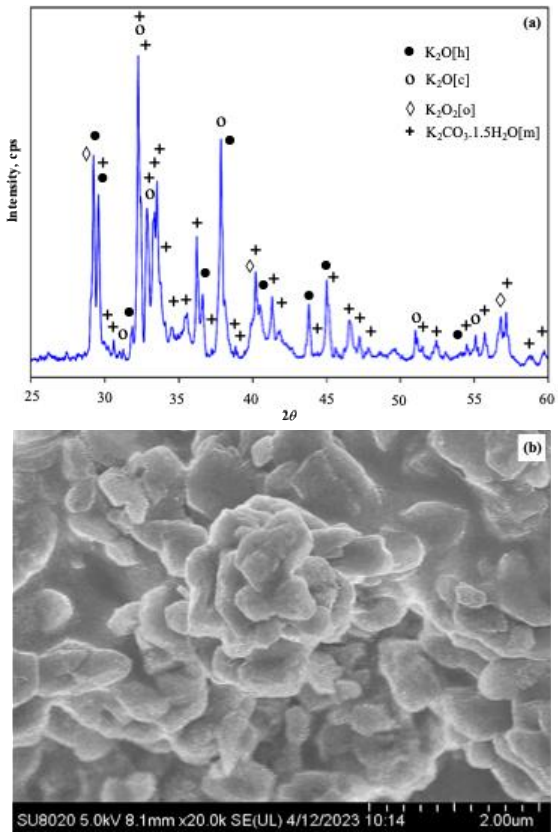


**Figure 3**. (a)XRD patterns and (b) FESEM micrograph at 20000 magnification of $K_2O$-ChiT calcined at 700 °C for 2h

**Table 1**. Nitrogen adsorption-desorption and Hammet analyses of $K_2O$-ChiT

| Parameter | | Unit | Results |
|---|---|---|---|
| Surface area | | $m^2/g$ | 6.784 |
| Average pore diameter | | nm | 17.75 |
| Pore volume | | $cm^3/g$ | 0.039 |
| Hammet analysis | Total basicity | mmol/g | 1.346 |
| | Total acidity | mmol/g | 1.515 |

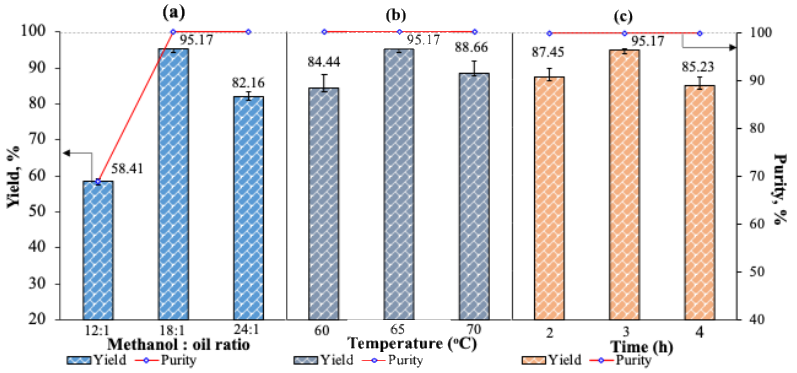


**Figure 4**. The effect of (a) methanol to oil ratio, (b) reaction temperature and (c) reaction time towards transesterification reaction catalysed by $K_2O$-ChiT

**Optimization of reaction condition**

The optimization of transesterification parameters was carried out by systematically varying the methanol-to-oil molar ratio, reaction temperature, and reaction time, as presented in **Figure 4**. These parameters play a critical role in determining biodiesel yield due to their influence on reaction equilibrium, kinetics, and mass transfer behaviour. As shown in **Figure 4a**, increasing the methanol to oil ratio from 12:1 to 18:1 resulted in a significant enhancement in biodiesel yield and purity. This trend can be attributed to the reversible nature of the transesterification reaction, where excess methanol shifts the equilibrium toward the formation of fatty acid methyl esters (FAME). However, a further increase to 24:1 led to a slight decrease in yield. This decline is likely due to the dilution Increasing methanol ratios have improved the reactant solubility and conversion, but excess methanol results in phase separation, and an abundance of methanol on the active site which promotes backward reactions, thereby reducing the overall conversion efficiency [23].

The effect of reaction temperature is illustrated in **Figure 4b**, where the biodiesel yield increased with temperature up to an optimum of 65 °C. This can be explained by enhanced molecular collisions and reduced viscosity of the reaction mixture, which improves mass transfer between immiscible phases. At temperatures above 65 °C, a marginal decrease in yield was observed. This behaviour is likely associated with partial methanol evaporation, even under reflux conditions, leading to a reduction in the effective methanol concentration in the reaction system [24]. Additionally, excessively high temperatures may affect catalyst stability and promote side reactions, contributing to the observed decline.

**Figure 4c** shows the influence of reaction time on biodiesel production. The yield increased progressively from 2 h to 3 h, indicating that sufficient time is required to achieve near-complete conversion of triglycerides. However, extending the reaction time to 4 h did not result in further improvement and instead caused a slight reduction in yield. This phenomenon may be attributed to the establishment of reaction equilibrium and the possible occurrence of reverse reactions thus reducing overall yield [23].

Overall, the optimal conditions were determined to be a methanol to oil ratio of 18:1, reaction temperature of 65 °C, and reaction time of 3 h, under which the catalyst achieved a biodiesel yield of approximately 95%. These optimised parameters reflect a balance between thermodynamic and kinetic factors, as well as efficient utilisation of the bifunctional acid–base active sites of the $K_2O$-ChiT catalyst. The presence of both acidic and basic sites likely facilitates simultaneous esterification and transesterification, contributing to the high catalytic performance observed.

**Conclusion**

In conclusion, the superior performance of the chitosan-based catalyst is supported by its structural and chemical properties. XRD analysis reveals the formation of multiple potassium species, including potassium oxides and potassium carbonate sesquihydrate, indicating strong interactions between potassium ions and chitosan's functional groups. These potassium compounds act as active sites that efficiently catalyse the transesterification of WCO. The catalyst's porous, brain-like morphology with interconnected ridges and pore channels facilitates reactant diffusion, enhancing catalytic activity as observed in FESEM images. Although the BET surface area is moderate due to some pore blockage, the presence of mesopores helps improve reactant accessibility. Hammett titration suggests bifunctional acidity and basicity with a balanced amount of acid (1.515 mmol/g) and base (1.346 mmol/g) sites, which is critical for processing low-quality feedstocks by

facilitating both esterification of free fatty acids and transesterification of triglycerides, thereby reducing soap formation and increasing biodiesel yield. The combined effect of accessbile potassium active sites by the enhanced porosity, and balanced acidity-basicity results in exceptional catalytic performance, achieving a biodiesel yield of 95.17%. Leaching and recyclability studies were not conducted in this work and will be addressed in future studies.

**Acknowledgement**

This work was supported by the Universiti Teknologi Malaysia through UTM Fundamental Research Grant (UTMFR)(Q.J130000.3854.22H42) and financial support (Nor Badariah binti Talib) from Yayasan Sultan Iskandar Johor.

**References**

1. Laskar, I. B., Changmai, B., Gupta, R., Shi, D., Jenkinson, K. J., Wheatley, A. E. H., and Rokhum, L. (2021). A mesoporous polysulfonic acid-formaldehyde polymeric catalyst for biodiesel production from *Jatropha curcas* oil. *Renewable Energy*, 173: 415-421.
2. Roy, T., Agarwal, A. K., and Sharma, Y. C. (2021). A cleaner route of biodiesel production from waste frying oil using novel potassium tin oxide catalyst: A smart liquid-waste management. *Waste Management*, 135: 243-255.
3. Ganesan, V., and Kim, J. (2020). Multi-shelled $CoS_2$-$MoS_2$ hollow spheres as efficient bifunctional electrocatalyst for overall water splitting. *International Journal of Hydrogen Energy*, 45:13290-13299.
4. Sathyan, A., Deng, L., Loman, T., and Palmans, A. R. A. (2023). Bioorthogonal catalysis in complex meida: consequences of using polymeric scaffold materials on catalyst stability and activity. *Catalysis Today*, 418: 114116.
5. Dohendou, M., Pakzad, K., Nezafat, Z., Nasrollahzadeh, M., and Dekamin, M. G. (2021). Progresses in chitin, chitosan, starch, cellulose, pectin, alginate, gelatin, and gum based (nano) catalyst for the Heck coupling reactions: A review. *International Journal of Biological Macromolecule*, 192:771-819.
6. Deng, J., Li, X., Liu, Y., Zeng, G., Liang, J., Song, B., and Wei, X. (2018). Alginate-modified biochar derived from Ca(II)-impregnated biomass: excellent anti-interference ability for Pb(II) removal. *Ecotoxicology and Environmental Safety*, 165: 211-218.
7. Cheryl-Low, Y. I., Theam, K. I., and Lee, H. V. (2015). Alginate-derived solid acid catalyst for esterification of low-cost palm fatty acid distillate. *Energy Conversion and Management*, 106: 932-940.
8. Fereidooni, L., Abbaspourrad, A., and Enayati, M. (2021). Electrolytic transesterification of waste frying oil using $Na^+$/zeolite–chitosan biocomposite for biodiesel production. *Waste Management*, 127, 48-62.
9. Sutirman, Z. A., Rahim, E. A., Sanagi, M. M., Abd Karim, K. J., and Ibrahim, W. A. W. (2020). New efficient chitosan derivative for Cu (II) ions removal: Characterization and adsorption performance. *International Journal Biological Macromolecules,* 153, 513-522.
10. Al-Sakkari, E. G., Attia, N. K., Habashy, M. M., Abdeldayem, O. M., Mostafa, S. R., El-Sheltawy, S. T., Abadir, M. F., Mostafa, M. K., Rene, E. R., and Elnashaie, S. S. E. H. (2021). A bifunctional alginate-based composite for catalyzing one-pot methyl esters synthesis from waste cooking oil having high acidity. *Fuel*, 306: 121637.
11. Takase, M., Bryant, I. M., Essandoh, P. K., and Amankwa, A. E. K. (2023). A comparative study on performance of KOH and 32%KOH/$ZrO_2$-7 catalyst for biodiesel via transesterification of waste adansonia digitata oil. *Green Technology Sustainability*, 1: 100004.
12. Lai, F., Yan, F., Wang, P., Wang, S., Li, S., and Zhang, Z.(2020). Highly efficient conversion of cellulose into 5-hydroxymethylfurfural using temperature-responsive $Ch_nH_{5-n}CeW_{12}O_{40}$ (n=1-5) catalyst. *Chemical Engineering Journal,* 396, 125282.
13. Hao, G., Hu, Y., Shi, L., Chen, J., Cui, A., Weng, W., Osako, K. (2021). Physicochemical characteristic of chitosan from swimming crab (*Portunus trituberculatus*) shells prepared by subcritical water pretreatment. *Scientific Reports,* 11:1646.
14. Han, X., Zheng, Z., Yu, C., Deng, Y., Ye, Q., Niu, F., Chen, Q., Pan, W., and Wang, Y. (2022). Preparation, characterization and antibacterial activity of new ionized chitosan. *Carbohydrate Polymers*, *290*, 119490.
15. Yu, D., Basumatary, I. B., Kumar, S., Ye, F., and Dutta, J. (2023). Chitosan modified with bio-extract as an antibacterial coating with UV filtering feature. *International Journal of Biological Macromolecules*, *230*, 123145.
16. Huamani-Palomino, R.G., Jacinto, C.R., Alarcon, H., Mejia, I.M., Lopez, R.C., Silva, D.O., Cavalheiro, E.T.G., Venancio, T., Davalos, J. Z., and Valderrama, A.C. (2019). Chemical modification of alginate with cysteine and its application for the removal of Pb(II) from aqueous solutions. *International Journal of Biological Macromolecules*, *129,* 1056-1068.
17. Shaari, N., and Kamaruddin, S.K. (2020). Sodium alginate/alumina composite biomembrane preparation and performance in DMFC application. *Polymer Testing, 81*,

106183.
18. Rukchonlatee, S., and Siriphannon, P. (2023). Facile preparation of montmorillonite/ crosslinked chitosan containing potassium nitrate nanocomposites as eco-friendly slow release fertilizers. *Journal of Polymers and the Environment*, 1-12.
19. Ciarleglio, G., Cinti, F., Toto, E., and Santonicola, M.G. (2023). Synthesis and characterization of alginate gel beads with embedded zeolite structures as carriers of hydrophobic curcumin. *Gels, 9,* 714.
20. Wulandri, W., Islami, D.M., Wellia, D.V., Emriadi, E., Siasc, V., and Jamarun, N. (2023). The effects of alginate concentration on crystallinity, morphology, and thermal stability properties of hydroxyapatite/alginate composite. *Polymers, 15,* 614.
21. Kulig, D., Zimoch-Korzycka, A., Jarmoluk, A., and Marycz, K. (2016). Study on alginate-chitosan complex formed with different polymers ratio, *Polymers,* 8: 5.
22. Cai, T., Chen, X., Tang, H., Zhou, W., Wu, Y., and Zhao, C. (2021). Unraveling the disparity of $CO_2$ sorption on alkali carbonates under high hu midity. *Journal of $CO_2$ Utilization,* 53, 101737.
23. Johari, S. A. M., Farid, M. A. A., Ayoub, M., Rashidi, N. A., and Andou, Y. (2024). Optimization and kinetic studies for biodiesel production from dairy waste scum oil via microwave assisted transesterification. *Environmental Technology & Innovation,* 34, 103580.
24. Zuhanee, M. K. A., Rahman, M. M., Hassan, M. M., Hossain, M. I., Ghos, B. C., Rana, G. M., Hossain, M. S., Ahmed, N., Rahman, M. N., and Yeasmin, M. S. (2025). Production, character zation and yield optimization of biodiesel from waste neem *Melia azadirachta* seeds available in Bangladesh. *Scientific Reports,* 15, 33913.